The Journal of Chemical Physics

Nonequilibrium atomistic molecular dynamics simulation of tubular nanomotor propelled by bubble propulsion

Cite as: J. Chem. Phys. **151**, 024103 (2019); https://doi.org/10.1063/1.5109101
Submitted: 06 May 2019 . Accepted: 11 June 2019 . Published Online: 10 July 2019

Viet Hoang Man, Mai Suan Li, Junmei Wang, Philippe Derreumaux, and Phuong H. Nguyen

The Journal of Chemical Physics ARTICLE scitation.org/journal/jcp

Nonequilibrium atomistic molecular dynamics simulation of tubular nanomotor propelled by bubble propulsion

Cite as: J. Chem. Phys. 151, 024103 (2019); doi: 10.1063/1.5109101
Submitted: 6 May 2019 • Accepted: 11 June 2019 •
Published Online: 9 July 2019

Viet Hoang Man,[1] Mai Suan Li,[2,3] Junmei Wang,[1] Philippe Derreumaux,[4,5,a)] and Phuong H. Nguyen[3,6,7,a)]

AFFILIATIONS

[1]Department of Pharmaceutical Sciences, School of Pharmacy, University of Pittsburgh, Pittsburgh, Pennsylvania 15213, USA
[2]Institute of Physics, Polish Academy of Sciences, Al. Lotnikow 32/46, 02-668 Warsaw, Poland
[3]Institute for Computational Science and Technology, SBI Building, Quang Trung Software City, Tan Chanh Hiep Ward, District 12, Ho Chi Minh City, Vietnam
[4]Laboratory of Theoretical Chemistry, Ton Duc Thang University, Ho Chi Minh City, Vietnam
[5]Faculty of Pharmacy, Ton Duc Thang University, Ho Chi Minh City, Vietnam
[6]CNRS, Université de Paris, UPR 9080, Laboratoire de Biochimie Théorique, 13 rue Pierre et Marie Curie, F-75005, Paris, France
[7]Institut de Biologie Physico-Chimique, Fondation Edmond de Rotschild, PSL Research University, Paris, France

[a)]**Authors to whom correspondence should be addressed:** philippe.derreumaux@tdtu.edu.vn and nguyen@ibpc.fr

ABSTRACT

We develop a molecular nanoscaled model for tubular motors propelled by bubble propulsion. The motor is modeled by a carbon nanotube, and the bubble is represented by a particle interacting with water by a time-dependent potential. Effects of liquid viscosity, fuel concentration, geometry, and size of the tube on the performance of the motor are effectively encoded into two parameters: time scales of the bubble expansion and bubble formation. Our results are qualitatively consistent with experimental data of much larger motors. Simulations suggest that (i) the displacement of the tube is optimized if two time scales are as short as possible, (ii) the compromise between the performance and fuel consumption is achieved if the bubble formation time is shorter than the velocity correlation time of the tube, (iii) the motor efficiency is higher with slow expansion, short formation of the bubble than fast growth but long formation time, and (iv) the tube is propelled by strong forces on the order of mN, reaching high speeds up to ~60 m/s. Our simulation may be useful for refining and encouraging future experimental work on nanomotors having the size of a few nanometers. The tiny size and high speed motors could have great potential applications in real life.

I. INTRODUCTION

In recent years, remarkable progress has been made in the development and application of self-propelled micro/nanomotors. These machines exhibit great potential applications in various fields, such as environment,[1] food industry,[2] and biomedicine.[3] Basically, a spatial field gradient is created across the structures, inducing the movement from high to low fields. Various energy sources, such as ultrasound, motile microorganisms, chemical, and biochemical reactions, have been used to generate such a field gradient. In addition, motors with various shapes, such as rods, Janus spheres, and tubes, have been fabricated.[4–7] Among these, bubble-driving tubular motors are most notable for their small size, light weight, strong driving force but low energy consumption. They possess a unique inner hollow, allowing for efficient catalytic, chemical, and biochemical reactions to take place inside the tube.[4,7,8] The reactions produce gas molecules, which then nucleate and form bubbles. The bubbles diffuse and then exit from one open end of the tube, propelling the tube to move in the opposite direction. This mechanism results in the unique stop-and-go behavior of bubble-propelled

motors.[9] While experimental studies have been extensively focusing on the fabrication, optimization, and demonstration for proof-of-concept applications of the motors, theoretical approaches are much behind. Most of the theoretical studies employ the continuum mechanics or Langevin dynamics simulations to describe the motion of motors.[10–24] These studies provide valuable insights into macroeffects, such as confinement, shape, size, external fields, liquid concentration, and viscosity on the motion of motors. However, we have not seen in the literature any all-atom molecular dynamics (MD) simulations aimed at studying the self-propelled mechanism at the molecular level. In addition, there are no experimental models having the size of a few nanometers. Given the difficulty and expense in the fabrication and optimization motors, especially at nanoscales, it is highly desirable to have MD studies, which would allow for a thorough understanding of the physics of the bubble-propelled mechanism in detail, prior to experimental work. With this in mind, the core aim of this work is twofolds: (i) develop a nanoscaled molecular model for bubble-propelled tubular motors and (ii) carry out atomistic nonequilibrium MD simulations with this model to study how its performance depends on the bubble expansion time in the liquid after exiting the tube, and the period of formation of two consecutive bubbles. Our results can qualitatively explain current experimental results, and make a prediction on the speed and propel force of very small nanomotors. This could be helpful for optimizing the balance between the performance and fuel consumption, thus designing more powerful tiny motors.

II. THE MODEL AND SIMULATION DETAILS

Our model consists of a carbon nanotube (CNT) and a bubble attached to one end of the tube. A bubble is represented by a low mass particle which does not interact with CNT but interacts with surrounding liquid atoms by a time-dependent Lennard-Jones potential of the following form:

$$V[r,\sigma(t)] = 4\epsilon\left[\left(\frac{\sigma(t)}{r}\right)^{12} - \left(\frac{\sigma(t)}{r}\right)^{6}\right], \quad (1)$$

where r is the distance between the bubble particle and a liquid atom, and $R(t) \equiv \sigma(t)$ is the bubble radius. The repulsive potential creates an empty cavity, mimicking a bubble in the liquid. This

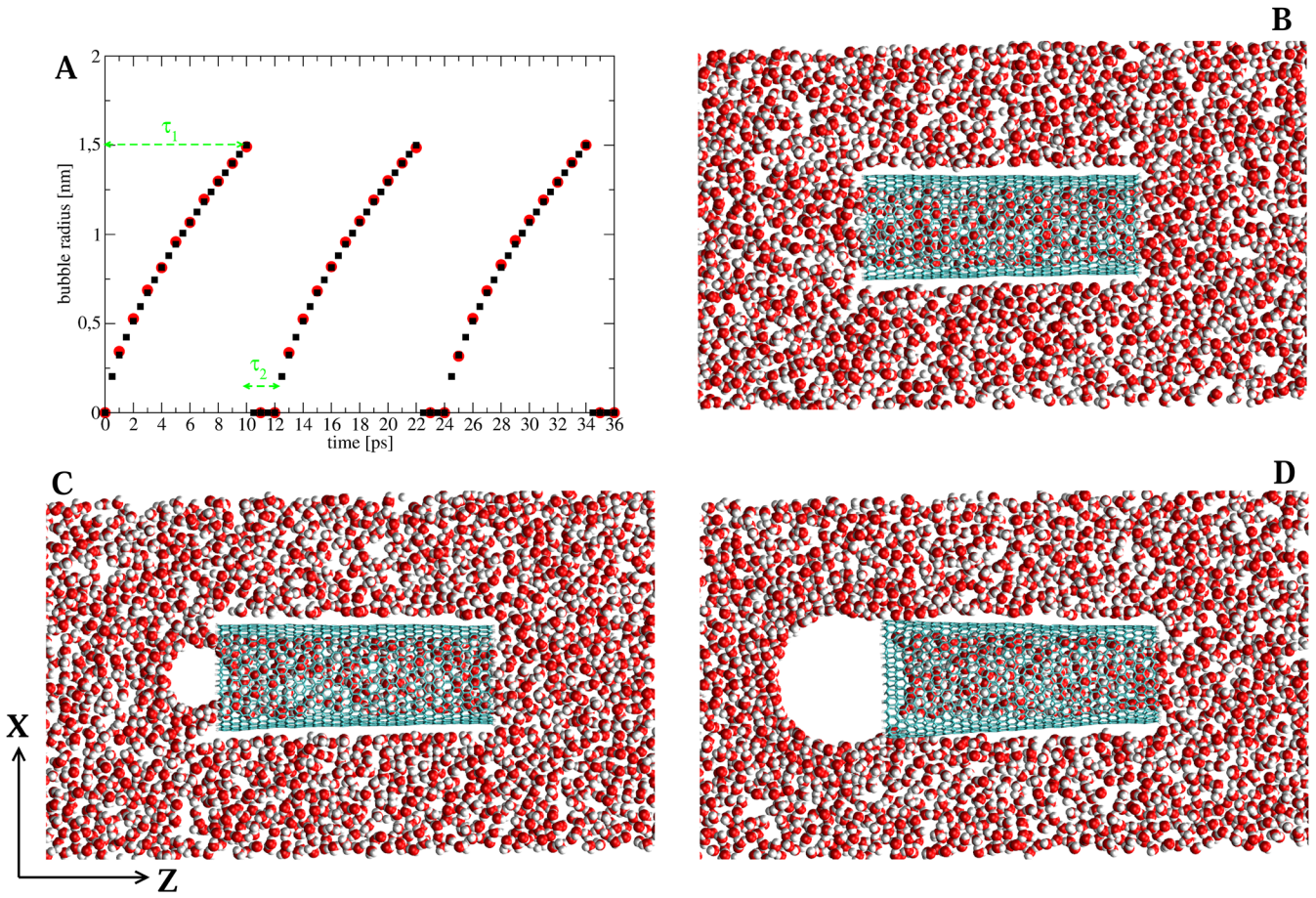

FIG. 1. (a) Time-evolution of the bubble radius obtained by Eqs. (2) and (3) (black) and simulation (red) for (τ_1, τ_2) = (10,2) ps (green). (b) The cross section XOZ of the initial structure of the system. (c) and (d) show the snapshots during the bubble expansion and when the bubble is fully grown. For clarity, only the first three bubble expansion periods are shown in (a).

bubble model has been developed and applied to study effects of the stable bubble cavitation on the amyloid fibril and lipid membrane models,[25,26] and to verify the Rayleigh-Plesset (RP) equation for the description of the dynamics of nanosized bubbles.[27] The bubble growth/shrinkage is generally described by the Rayleigh-Plesset (RP) equation.[27–29] Assuming that the bubble radius increases as $R(t) \sim t^m$, then for small radius, it can be derived from the RP equation that $m = 2/3$.[7] Thus, for our nanosized bubble, the time-dependent bubble radius is expressed as a function of the following form:

$$R(t) = \begin{cases} R_{\max}\left(\frac{t}{\tau_1}\right)^{2/3}, & t \le \tau_1, \quad (2) \\ 0, & \tau_1 < t \le \tau_1 + \tau_2. \quad (3) \end{cases}$$

Equation (2) describes the expansion of a bubble from initial radius $R(0) = 0$ to the maximum value $R_{\max}$ at time τ_1. Equation (3) mimics the detachment of the bubble from the CNT after full growth; i.e., there is no bubble within time $\tau_1 < t \le \tau_1 + \tau_2$. In other words, τ_2 is the delay time for forming a next bubble. After that, a new bubble appears and grows according to Eq. (2), then disappears again according to Eq. (3). This process is repeated during the simulation and illustrated in Fig. 1(a).

Having defined the model, we carry out MD simulations using a CNT with a length and radius of 6 nm and 1 nm, respectively. The bubble is allowed to expand to $R_{\max} = 1.5$ nm. The all-atom OPLS force field and TIP3P water model[30] are employed to describe the CNT and liquid, respectively. The repulsive strength $\epsilon = 20$ kJ/mol [Eq. (1)] is simply large enough to maintain the cavity. The CNT is initially placed at the center of a rectangle box with edge lengths $(L_x, L_y, L_z) = (8, 8, 14)$ nm, and the first principal axis is aligned along the Z-axis [Fig. 1(b)]. To determine the time scale of the bubble expansion, τ_1, we carry out an MD simulation of only TIP3P water, where an empty cavity with the radius of 1.5 nm is initially created in the box. This way, we obtain the collapse time scale of the cavity of ~10 ps, well-agreed with previous studies.[31,32] Assuming that the growth and collapse of a small bubble are symmetric, this suggests us to use the value $\tau_1 = 10$ ps in simulations. Because the properties of liquid and gas affect the speed of bubble expansion, and to effectively mimic this effect, we also carry out simulations with $\tau_1 = 20$ ps. The effect of the delay time is studied by varying the value of τ_2 in the range $\tau_2 = 0, \ldots, 30$ ps. For each parameter set, we carry out 10 trajectories, starting from different initial equilibrium states of the tube. The length of each trajectory is 500 ps.

The GROMACS simulation package[33] coupled to our bubble code is used for all the simulations. We suggest that the appropriate conditions for the simulations are constant volume with only the water coupled to the heat bath at a temperature of 280 K using the Berendsen coupling method[34] with a temperature coupling constant of 0.1 ps. This ensures that directional motion of the CNT is not suppressed due to the artificial rescale of the velocities of atoms done by the coupling method. The equations of motion are integrated using the leapfrog algorithm with a small time step of 1 fs. The electrostatic interactions are calculated using the particle mesh Ewald method and a cutoff of 1.4 nm.[35] A cutoff of 1.4 nm is used for the van der Waals interactions. The nonbonded pair lists are updated every 5 fs. The use of small time step, more frequent update of the pair lists, and a large neighboring list ensures that temperature of the water is well-maintained.

III. RESULTS

Figure 1(a) shows the time-evolution of the bubble radius during the simulation for the case $\tau_1 = 10$ ps and $\tau_2 = 2$ ps. As expected, its behavior is similarly to the theoretical curve [Eqs. (2) and (3)]. The bubble starts to form at $t = 0$ ps at one end of the tube, then its radius increases [Fig. 1(c)] and reaches the maximum value of 1.5 nm at 10 ps [Fig. 1(d)]. During the next delay time of 2 ps, there is no bubble [Eq. (3)]. After that, a second bubble is formed, grown within the next 10 ps, and detached from the tube. This process is repeated over 500 ps, resulting in the enhanced motion of the tube. Indeed, Fig. 2 shows a typical trajectory of the center of mass of the tube in the XOZ plane. The tube starts initially at $(X, Z) = (4.2, 6.7)$ nm, then moves preferably along the Z-axis, and reaches $Z \approx 11$ nm, then moves along the opposite direction and ended up at $Z \approx 5.5$ nm. For a comparison, we also show the equilibrium trajectory, i.e., without bubble. Within 500 ps, the tube explores a very limited space, spanning between $3.5 < X < 4.2$ nm and $6 < Z < 7$ nm. We also show a trajectory with $\tau_1 = 10$ ps, but with longer delay time $\tau_2 = 6$ ps. As seen, it samples the space more efficiently than the equilibrium trajectory, but less efficiently than the counterpart with shorter delay time $\tau_2 = 2$ ps. Figure 3(a) shows the mean-square-displacement (MSD) of the tube propelled by the bubble with expansion time $\tau_1 = 10$ ps and with various delay times τ_2. The corresponding diffusion coefficients D are shown in Fig. 3(b). As seen, given a value of τ_1, the longer delay time between the formation of two consecutive bubbles, the shorter displacement of the tube. With $\tau_1 = 10$ ps and $\tau_2 = 0$ ps, i.e., the bubble is continuously formed, the tube achieves a displacement of ~70 nm^2 within 500 ps with the diffusion coefficient $D = 25 \times 10^{-5}$ cm^1 s^{-1}. With delay times $\tau_2 = 2$ ps and $\tau_2 = 4$ ps, the tube moves slightly slower with $D = 22 \times 10^{-5}$cm^1 s^{-1} and $D = 20 \times 10^{-5}$ cm^1 s^{-1}, respectively. With $\tau_2 = 6$ ps, the displacement is shorter with MSD = 40 nm^2 and

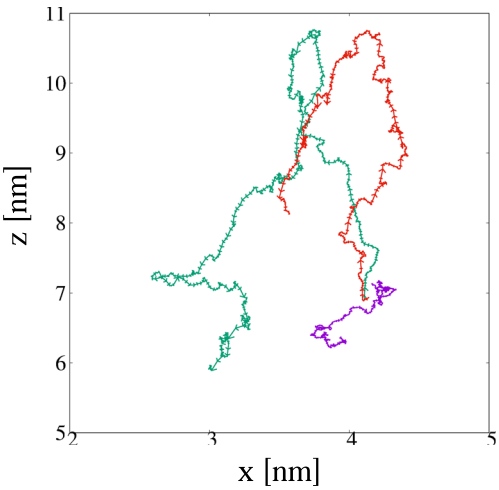

FIG. 2. The time-evolution of the center of mass coordinates (X, Z) of the CNT propelled by the bubble with $(\tau_1, \tau_2) = (10, 0)$ ps (green) and $(\tau_1, \tau_2) = (10, 6)$ ps (red). The equilibrium trajectory, i.e., no bubble propulsion, is shown in pink. The arrow indicates the direction of motion. Initially, the main axis of the tube is aligned along the Z-axis.

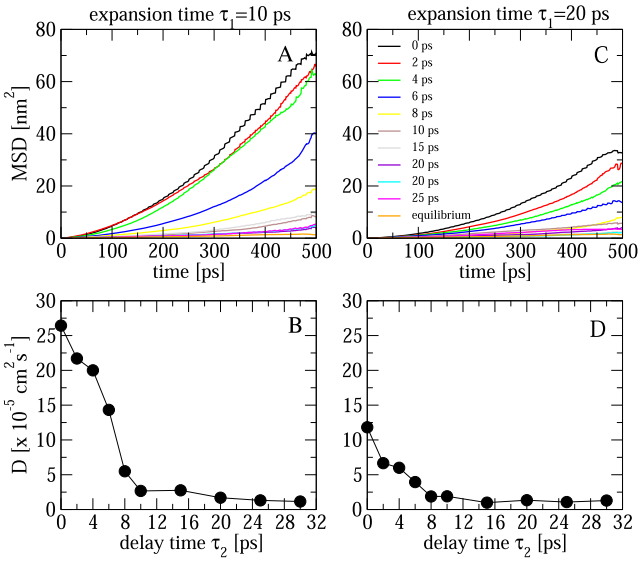

FIG. 3. The mean square displacements of the CNT propelled by the bubble with expansion time τ_1 = 10 ps (a) and τ_1 = 20 ps (c). For each case, shown are results obtained by various delay times τ_2 = 0, 2, . . ., 25 ps. The diffusion coefficients corresponding to displacements shown in (a) and (b) are shown in (c) and (d), respectively.

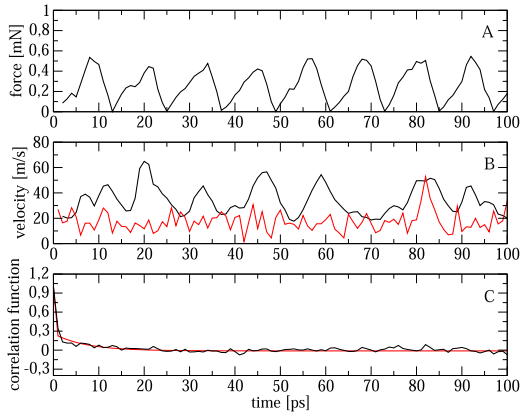

FIG. 4. Time evolution of force acting on water by the bubble propulsion (a) and velocity of the center of mass of the tube [(b), red] during the simulation with τ_1 = 10, τ_2 = 2 ps. The equilibrium velocity and its autocorrelation function are shown in [(b), red] and [(c), black], respectively. An exponential fit is shown in [(c), red]. For clarity, only the first 100 ps data are shown.

$D = 14 \times 10^{-5}$ cm^1 s^{-1}. However, with τ_2 = 8 ps, the tube moves much slower with $D = 5 \times 10^{-5}$ cm^1 s^{-1}, and only achieves a displacement of ~ 20 nm^2. For $\tau_2 > 8$ ps, the motion is not much enhanced as compared to the case without bubble propulsion. Similar results, but with slower expansion time τ_1 = 20 ps, are shown in Figs. 3(c) and 3(d). Compared to the case τ_1 = 10 ps, it is clear that the slower expansion of the bubble, the smaller diffusion coefficient, and the shorter displacement are achieved by the tube, given the same delay time τ_2. However, in both cases, the motion of the tube is not much enhanced if the delay time $\tau_2 > 8$ ps. An interesting question is that which strategy is better for a compromise between fuel consumption and enhanced motion: fast bubble expansion, long delay time, or slow bubble expansion but short delay time, given that $\tau_{1(\text{fast})} + \tau_{2(\text{slow})} = \tau_{1(\text{slow})} + \tau_{2(\text{fast})}$? Our results suggest that the latter strategy could be better. For example, with (τ_1 = 10, τ_2 = 10) ps, then $D = 2.5 \times 10^{-5}$ cm^1 s^{-1}, but with (τ_1 = 20, τ_2 = 0) ps, then $D = 15 \times 10^{-5}$ cm^1 s^{-1}.

To quantitatively explain the enhanced motion of the tube, we calculate the force that the bubble exerts on water and pushes the tube to move in the opposite direction. The result is shown in Fig. 4(a) for the case τ_1 = 10 ps and τ_2 = 2 ps. As seen, the force increases from 0 to ~0.6 mN upon the expansion of the bubble radius from 0 to 1.5 nm during t = 10 ps. This accelerates the motion of the tube, as indicated by the increase in the velocity of the center of mass from the equilibrium value of ~20 m/s to the maximum value of ~60 m/s [Fig. 4(b)]. During the delay time of 2 ps, i.e., no bubble propulsion, the motion is slowed down as indicated by the decrease in the velocity. However, the velocity is still higher than the equilibrium value. This is because the delay time of 2 ps is shorter than the velocity correlation time, as shown below; thus, the system is still not fully equilibrated before the next bubble propulsion. To explain why the motion of the tube is not significantly enhanced if $\tau_2 > 8$ ps, we calculate the autocorrelation function of the velocity of the tube center of mass from an equilibrium trajectory, i.e., without bubble propulsion, and the result is shown in Fig. 4(c). A fit of the data to an exponential function of the form $C(t) = A \exp(-t/\tau)$ results in the decay time τ = 8.2 ps. This suggests that the motions between two consecutive bubble propulsions are weakly correlated if $\tau_2 > 8.2$ ps. The tube is propelled by the bubble propulsion, but this enhanced motion is then thermally randomized and stopped, and the next propulsion starts again from a random state. This results in inefficient motion.

IV. DISCUSSION AND CONCLUDING REMARKS

We have developed a nanoscaled prototype molecular tubular motor propelled by bubble propulsion. We acknowledge that currently there is no single experimental motor whose size is comparable with our model; thus, our results cannot be compared directly to experiments. Encouragely, recent attempts have been made to reduce the size of motors to a few hundreds of nanometers,[36] and we believe that smaller size motors, down to a few nanometers will be available in the future, and results can be directly compared to our current data. Nevertheless, our model still can qualitatively confirm current results of much larger motors. Our model contains two time scales: bubble expansion, τ_1, and bubble formation, τ_2. In general, their values depend on various factors including gas properties (such as density, chemical components), surface tension, liquid properties (such as viscosity), geometry of the tube (such as cylinder, cone), size of the tube (such as length, diameter), position of the fuel source in the tube, and the external excitations (such as ultrasound, laser). Notably, τ_1 strongly depends on the liquid viscosity, that is, the higher viscosity, the slower bubble expansion, i.e., the longer τ_1, thus, slower motion as shown above. This result is consistent with experimental and theoretical studies which show that the velocity of

motors is inverse proportion to the liquid viscosity.[3,16,21,37–40] These studies also show that the velocity of motors is in direct proportion to the fuel concentration and length of the tube. This is also consistent with our simulation because the high fuel concentration and the long tube, i.e., the large reaction surface area, will increase the frequency of bubble formation; therefore, τ_2 is short, and the motion is increased as shown above. However, the too high concentration has very little influence on the velocity.[3] This situation corresponds to $\tau_2 \to 0$ in our model, showing that the velocity is reaching a maximum value, for a given value of τ_1. In summary, our simulations show that (i) to maximize the displacement of the tube given a time duration, both τ_1 and τ_2 must be as short as possible. This could be achieved by designing motor shapes that reduce the drag force, increasing the fuel concentration and surface reaction area. (ii) To obtain a compromise between the performance and fuel consumption of the motors, τ_2, however, does not have to be very short, unless it is shorter than the velocity correlation time of the tube. This is probably not significant for large micromotors whose velocity correlation time is anyways much longer than the bubble formation time. These two times are, however, on the picosecond time scale for nanoscaled motors, and the optimization of τ_2 is important. (iii) The motor efficiency is better with long τ_1 but short τ_2 than short τ_1 but long τ_2. This could be important for high viscous environment where one should focus more on the optimization of the fuel concentration. (iv) We show that the propel force of our nanosized motor is quite strong, around 0.6 mN, pushing the tube to the velocity up to ~60 m/s. This could be important for real applications, such as biomedicine, where the motors should be small but move fast enough to be able to cross the lipid membranes and deliver drugs to cells. We should mention that the maximum speed of one of the current fastest microtubular motors is ~10 mm/s,[41] much lower than the speed of our nanomotor. This is due to the fact that our tube is very small in size and thus hindered by very weak drag force, as compared to much larger experimental tubes hindered by much stronger drag forces. In addition, the bubble expelling frequency is very high in our simulation with a period of 2–20 ps, whereas the experimental period is 0.1–0.06 s.[37,42,43] Nevertheless, we should note that our results are just theoretical values obtained from our prototype model and cannot be compared directly to experimental data. We hope that in the future the computer power will be strong enough, allowing us to simulate more realistic systems with larger length and longer time scales such that the simulation results can be compared directly to experimental data. We also note that our model does not consider the effect of the bubble collapse on the motion of tube, although this aspect was recently examined by the experiment, showing that the motion could be enhanced.[44] Finally, the model will allow us to explore challenge issues, such as dynamics of the nanomotors in complex environments, including confinement and lipid membranes, and the cooperation of a large number of motors, which is important for drug delivery. These works are underway.

ACKNOWLEDGMENTS

This work was supported by the Department of Science and Technology at Ho Chi Minh City, Vietnam (Grant No. 10/2018/HD-KHCNTT), the CNRS, the Polish NCN (Grant No. 2015/19/B/ST4/02721), and the National Institutes of Health (Grant Nos. R01-GM079383, R21-GM097617, and P30-DA035778). The content is solely the responsibility of the authors and does not necessarily represent the official views of the National Institutes of Health or other funding organizations. Computational support from the IDRIS, CINES, TGCC centers (Project No. A0040710411), the Center for Research Computing of University of Pittsburgh, and the Extreme Science and Engineering Discovery Environment (Grant Nos. CHE090098, MCB170099, and MCB180045P) are acknowledged.

REFERENCES

[1] L. Soler, V. Magdanz, V. M. Fomin, S. Sanchez, and O. G. Schmidt, "Self-propelled micromotors for cleaning polluted water," ACS Nano **7**, 9611 (2013).
[2] A. Molinero-Fernandez, M. Moreno-Guzman, M. Lopez, and A. Escarpa, "Biosensing strategy for simultaneous and accurate quantitative analysis of mycotoxins in food samples using unmodified graphene micromotors," Anal. Chem. **89**, 10850 (2017).
[3] Z. Wu, Y. Wu, W. He, X. Lin, J. Sun, and Q. He, "Self-propelled polymer-based multilayer nanorockets for transportation and drug release," Angew. Chem., Int. Ed. **52**, 7000 (2013).
[4] J. Katuri, X. Ma, M. M. Stanton, and S. Sanchez, "Designing micro- and nanoswimmers for specific applications," Acc. Chem. Res. **50**, 2 (2017).
[5] L. Ren, W. Wang, and T. E. Mallouk, "Two forces are better than one: Combining chemical and acoustic propulsion for enhanced micromotor functionality," Acc. Chem. Res. **51**, 1948 (2018).
[6] T. Patino, X. Arque, R. Mestre, L. Palacios, and S. Sanchez, "Fundamental aspects of enzyme-powered micro- and nanoswimmers," Acc. Chem. Res. **51**, 2662 (2018).
[7] F. Zha, T. Wang, M. Luo, and J. Guan, "Tubular micro/nanomotors: Propulsion mechanisms, fabrication techniques and applications," Micromachines **9**, 78 (2018).
[8] B. Xu, B. Zhang, L. Wang, G. Huang, and Y. Mei, "Tubular micro/nanomachines: From the basics to recent advances," Adv. Funct. Mater. **28**, 1705872 (2018).
[9] Y. Mei, G. Huang, A. A. Solovev, E. B. Urena, I. Monch, F. Ding, T. Reindl, R. K. Y. Fu, P. K. Chu, and O. G. Schmidt, "Versatile approach for integrative and functionalized tubes by strain engineering of nanomembranes on polymers," Adv. Matter **20**, 4085 (2008).
[10] J. L. Anderson, "Colloid transport by interfacial forces," Ann. Rev. Fluid Mech. **21**, 61 (1989).
[11] R. Golestanian, T. B. Liverpool, and A. Ajdari, "Designing phoretic micro- and nano-swimmers," New J. Phys. **9**, 126 (2007).
[12] G. Ruckner and R. Kapral, "Chemically powered nanodimers," Phys. Rev. Lett. **98**, 150603 (2007).
[13] J. G. Gibbs and Y. P. Zhao, "Autonomously motile catalytic nanomotors by bubble propulsion," Appl. Phys. Lett. **94**, 163104 (2009).
[14] Y.-G. Tao and R. Kapral, "Swimming upstream: Self-propelled nanodimer motors in a flow," Soft Matter **6**, 756 (2010).
[15] H. A. Zambrano, J. H. Walther, and R. L. Jaffe, "Thermally driven molecular linear motors: A molecular dynamics study," J. Chem. Phys. **131**, 241104 (2009).
[16] J. Li, G. Huang, M. Ye, M. Li, R. Liu, and Y. Mei, "Dynamics of catalytic tubular microjet engines: Dependence on geometry and chemical environment," Nanoscale **3**, 5083 (2011).
[17] S. Ebbens, M. H. Tu, J. R. Howse, and R. Golestanian, "Size dependence of the propulsion velocity for catalytic Janus-sphere swimmers," Phys. Rev. E **85**, 020401 (2012).
[18] M. T. Manjare, B. Yang, and Y. P. Zhao, "Bubble driven quasioscillatory translational motion of catalytic micromotors," Phys. Rev. Lett. **109**, 128305 (2012).
[19] P. de Buyl and R. Kapral, "Phoretic self-propulsion: A mesoscopic description of reaction dynamics that powers motion," Nanoscale **5**, 1337 (2013).
[20] V. M. Fomin, M. Hippler, V. Magdanz, L. Soler, S. Sanchez, and O. G. Schmidt, "Propulsion mechanism of catalytic microjet engines," IEEE Trans. Robot **30**, 40 (2014).
[21] L. Li, J. Wang, T. Li, W. Songa, and G. Zhanga, "Hydrodynamics and propulsion mechanism of self-propelled catalytic micromotors: Model and experiment," Soft Matter **10**, 7511 (2014).

[22]J.-X. Chen, Y.-G. Chen, and Y.-Q. Ma, "Chemotactic dynamics of catalytic dimer nanomotors," Soft Matter **12**, 1876 (2016).
[23]D. S. Cambuia, M. Godoyc, and A. de Arruda, "Finite-size effects in simulations of self-propelled particles system," Physica A **467**, 129 (2017).
[24]L. Deprez and P. de Buyl, "Passive and active colloidal chemotaxis in a microfluidic channel: Mesoscopic and stochastic models," Soft Matter **13**, 3532 (2017).
[25]M. H. Viet, P. Derreumaux, and P. H. Nguyen, "Nonequilibrium all-atom molecular dynamics simulation of the ultrasound induced bubble cavitation and application to dissociate amyloid fibril," J. Chem. Phys. **145**, 174113 (2016).
[26]M. H. Viet, M. T. Phan, M. Li, P. Derreumaux, W. Junmei, N. T. Van-Oanh, P. Derreumaux, and P. H. Nguyen, "Molecular mechanism of the cell membrane pore formation induced by bubble stable cavitation," J. Phys. Chem. B **123**, 71 (2019).
[27]M. H. Viet, M. Li, P. Derreumaux, and P. H. Nguyen, "Rayleigh-Plesset equation of the bubble stable cavitation in water: A nonequilibrium all-atom molecular dynamics simulation study," J. Chem. Phys. **148**, 094505 (2018).
[28]Lord Rayleigh, "On the pressure developed in a liquid during the collapse of a spherical cavity," Phil. Mag. **34**, 94–98 (1917).
[29]M. S. Plesset, "The dynamics of cavitation bubbles," J. Appl. Mech. Trans. ASME **16**, 277–282 (1949).
[30]G. A. Kaminski, R. A. Friesner, J. Tirado-Rives, and W. L. Jorgensen, "Evaluation and reparametrization of the OPLS-AA force field for proteins via comparison with accurate quantum chemical calculations on peptides," J. Phys. Chem. B **105**, 6474–6487 (2001).
[31]J. Dzubiella, "Interface dynamics of microscopic cavities in water," J. Chem. Phys. **126**, 194504 (2007).
[32]F. Lugli, S. Hofinger, and F. Zerbetto, "The collapse of nanobubbles in water," J. Am. Chem. Soc. **127**, 8020 (2005).
[33]E. Lindahl, B. Hess, and D. van der Spoel, "GROMACS 3.0: A package for molecular simulation and trajectory analysis," J. Mol. Mod. **7**, 306–317 (2001).
[34]H. J. C. Berendsen, J. P. M. Postma, W. F. van Gunsteren, A. Dinola, and J. R. Haak, "Molecular-dynamics with coupling to an external bath," J. Chem. Phys. **81**, 3684–3690 (1984).
[35]T. Darden, D. York, and L. Pedersen, "Particle mesh Ewald: An $N\cdot\log(N)$ method for Ewald sums in large systems," J. Chem. Phys. **98**, 10089–10092 (1993).
[36]X. Ma, A. C. Hortelao, A. Miguel-Lopez, and S. Sanchez, "Bubble-free propulsion of ultrasmall tubular nanojets powered by biocatalytic reactions," J. Am. Chem. Soc. **138**, 13782 (2016).
[37]W. Gao, S. Sattayasamitsathit, J. Orozcoa, and J. Wang, "Highly efficient catalytic microengines: Template electrosynthesis of polyaniline/platinum microtubes," J. Am. Chem. Soc. **133**, 11862 (2011).
[38]W. Gao, S. Sattayasamitsathit, J. Orozcoa, and J. Wang, "Efficient bubble propulsion of polymer-based microengines in real-life environments," Nanoscale **5**, 8909 (2013).
[39]L. Wanga, T. Li, L. Li, J. Wang, W. Songa, and G. Zhanga, "Microrocket based viscometer," ECS J. Solid State Sci. Technol. **4**, S3020 (2015).
[40]L. Liu, T. Bai, Q. Chi, Z. Wang, S. Xu, Q. Liu, and Q. Wang, "How to make a fast, efficient bubble-driven micromotor: A mechanical view," Micromachines **8**, 267 (2017).
[41]S. Sanchez, A. N. Ananth, V. M. Fomin, M. Viehrig, and O. G. Schmidt, "Superfast motion of catalytic microjet engines at physiological temperature," J. Am. Chem. Soc. **133**, 14860 (2011).
[42]A. A. Solovev, Y. Mei, E. B. Urena, G. Huang, and O. G. Schmidt, "Catalytic microtubular jet engines self-propelled by accumulated gas bubbles," Small **5**, 1688 (2009).
[43]A. A. Solovev, S. Sanchez, M. Pumera, Y. F. Mei, and O. G. Schmidt, "Magnetic control of tubular catalytic microbots for the transport, assembly, and delivery of micro-objects," Adv. Funct. Mater. **20**, 2430 (2010).
[44]L. Wang, L. Chen, J. Zhang, J. Duan, L. Wang, Z. Silber-Li, X. Zheng, and H. Cui, "Efficient propulsion and hovering of bubble-driven hollow micromotors underneath an air–liquid interface," Langmuir **34**, 10426 (2018).